

The influence of the land surface on hydrometeorology and ecology: new advances from modeling and satellite remote sensing

Venkat Lakshmi, Seungbum Hong, Eric E. Small and Fei Chen

ABSTRACT

The importance of land surface processes has long been recognized in hydrometeorology and ecology for they play a key role in climate and weather modeling. However, their quantification has been challenging due to the complex nature of the land surface amongst other reasons. One of the difficult parts in the quantification is the effect of vegetation that are related to land surface processes such as soil moisture variation and to atmospheric conditions such as radiation. This study addresses various relational investigations among vegetation properties such as Normalized Difference Vegetation Index (NDVI), Leaf Area Index (LAI), surface temperature (TSK), and vegetation water content (VegWC) derived from satellite sensors such as Moderate Resolution Imaging Spectroradiometer (MODIS) and EOS Advanced Microwave Scanning Radiometer (AMSR-E). The study provides general information about a physiological behavior of vegetation for various environmental conditions. Second, using a coupled mesoscale/land surface model, we examine the effects of vegetation and its relationship with soil moisture on the simulated land-atmospheric interactions through the model sensitivity tests. The Weather Research and Forecasting (WRF) model was selected for this study, and the Noah land surface model (Noah LSM) implemented in the WRF model was used for the model coupled system. This coupled model was tested through two parameterization methods for vegetation fraction using MODIS data and through model initialization of soil moisture from High Resolution Land Data Assimilation System (HRLDAS). Finally, this study evaluates the model improvements for each simulation method.

Key words | land-atmosphere interactions, satellite remote sensing, soil moisture, vegetation, WRF model

Venkat Lakshmi (corresponding author)
Seungbum Hong
Department of Geological Sciences,
University of South Carolina,
Columbia SC 29201,
USA
E-mail: venkat-lakshmi@sc.edu

Eric E. Small
Department of Geological Sciences,
University of Colorado,
Boulder, CO 80309,
USA

Fei Chen
Research Application Lab,
National Center for Atmospheric Research,
Boulder, CO 80307,
USA

INTRODUCTION

The land surface greatly influences the near-surface atmosphere and the studies of the land and atmospheric interactions have provided critical information for numerical weather and climate modeling. One of the most critical processes is the water cycle, namely the influence of vegetation on evapotranspiration, soil moisture and sensible heat fluxes. For example, the variations of surface energy and moisture fluxes by soil and vegetation surface are strongly related to thunderstorm formation (Pielke 2001). Meanwhile,

climate and meteorological variations impact land surface characteristics such as vegetation distribution, energy balance, and watershed hydrology (e.g., Small & Kurc 2003; Weiss *et al.* 2004). The hydraulic properties of soil and vegetation play a key role in the variability of surface moisture. For example, the soil type with varying hydraulic conductivities determines the soil moisture, and vegetation properties such as canopy height, leaf amount, and root zone determines vegetation transpiration. Soil and vegetation

also directly interact with each other. For example, properties of the root zone such as its depth and width have an impact on vertical moisture distribution in soil layers (Kleidon & Heimann 1998; Pielke 2001). For over a decade the coupled (land and atmosphere) modeling system has been developed to provide improved simulations in conjunction with various field projects. However, quantification of vegetation behavior has been the most difficult aspect because of its complex relationships with atmosphere as well as other land surface processes.

In order to evaluate the contribution of vegetation to the land and atmospheric interactions, this study addresses investigations of the relationships among vegetation properties, using satellite-derived data: normalized difference vegetation index (NDVI), leaf area index (LAI), vegetation water content (VegWC), and skin surface temperature (T_s). The main purpose of this is to evaluate the meteorological effect of satellite derived VegWC and the prospect for its application to numerical forecasting models through the following relational analyses with the other variables: (1) the relationship between LAI and VegWC, (2) between NDVI and VegWC, and (3) between NDVI, T_s , and VegWC. For these analyses, three different hydroclimatic regions in North America are selected: semiarid, intermediate, and humid regions. Next, this study uses simulations from a land-atmosphere coupled model to compare the simulated fluxes to their observed counterparts. We use two different vegetation parameterizations and soil moisture initialization to check the validity of the model.

DATA AND METHOD

Study areas

Three regions have been selected to examine the spatial variations of the land surface variables (Figure 1): (a) the North American Monsoon System (NAMS) region; (b) the South Great Plains (SGP) region, and (c) the Little River Watershed in Tifton, Georgia. The geographic latitude and longitude of their center points are 33.5 N and 107.5 W, 36.5 N and 100.0 W, and 32.4 N and 84.0 W, respectively. The NAMS region has been the focus of numerous studies on the interactions between meteorology, vegetation, and land surface fluxes (Kurc & Small 2004; Weiss *et al.* 2004). For comparison of climate changes in the NAMS region with other regions, the International H2O Project (IHOP_2002) has been undertaken since 2002 (Weckwerth *et al.* 2004) in the SGP region. The Little River Watershed region around Tifton, Georgia as one of the highly vegetated regions in east coast areas has been a subject for soil moisture research. This region has a humid climate and denser vegetation than the NAMS and SGP regions. Because of the short-term but very frequent rainfall events in summer, it has large inundated areas with mixed forests (Bosch *et al.* 1999). Satellite data have been processed in equal-sized areas (500 km × 500 km) for those study regions, and they are referred to as follows: NAMS, IHOP, and Tifton, GA. Figure 1 shows typical climatic trends of the three regions. The NAMS region is relatively dry with relatively low

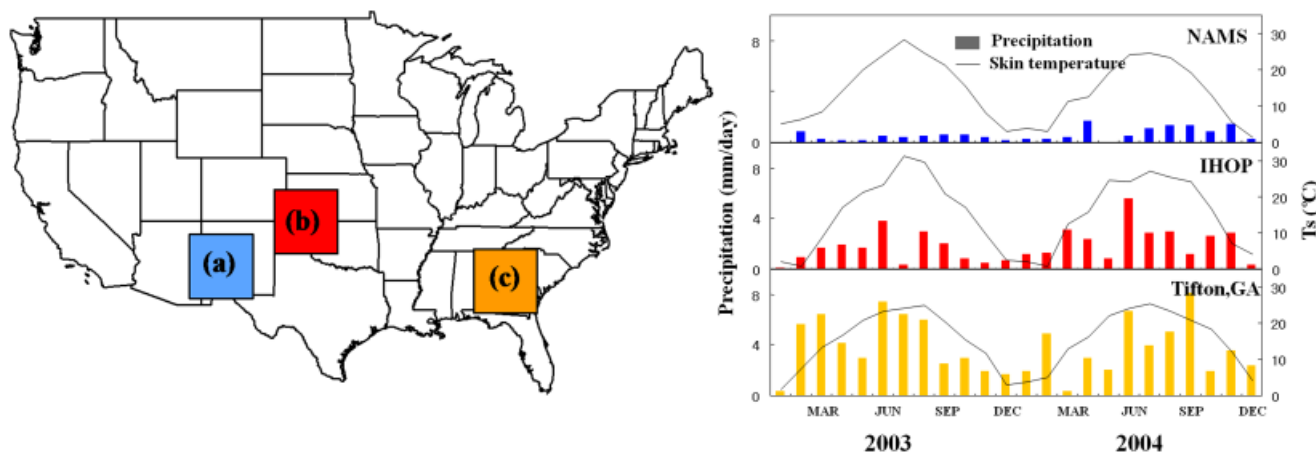


Figure 1 | The three study regions and the climograph of each region with precipitation and surface temperature (data from www.cdc.noaa.gov).

vegetation amount. Major types of vegetation in this region are shrublands with limited grasslands and crops. The IHOP region, in contrast, shows a relatively more humid climate with more vegetation which is grasslands, crops, and limited trees. Tifton, GA is highly vegetated with mixed forest (e.g., pines and hardwoods) and crops (e.g., peanuts and cotton), showing wet and humid climate with highly frequent rainfalls. Of the three study regions, the IHOP region was especially selected for the coupled model tests due to the availability of ground observations.

Satellite data

We obtained two different types of satellite data: Moderate Resolution Imaging Spectroradiometer (MODIS) and Advanced Microwave Scanning Radiometer for Earth Observing System (AMSR-E). MODIS flies onboard the Terra and Aqua satellite platforms, which were launched on 18 December 1999 and on 4 May 2002, respectively, and only Terra MODIS data were utilized for this study. The algorithms of the MODIS land data are available at the MODIS website (<http://modis.gsfc.nasa.gov>), and we downloaded the land data, surface reflectance, NDVI, Ts, and LAI from the Land Processes Distributed Active Archive Center (LPDAAC) website (<http://edcdacc.usgs.gov>) for this study. The AMSR-E instrument on the NASA EOS Aqua satellite provides global passive microwave measurements of terrestrial, oceanic, and atmospheric variables for the investigation of global water and energy cycles (Njoku *et al.* 2003; Shibata *et al.* 2003). The AMSR-E observed brightness temperatures at the 6, 10 and 18 GHz are used in conjunction with a radiative transfer model to simultaneously retrieve the surface soil moisture, Ts and VegWC. The radiative transfer model is run in an iterative fashion and these three variables are adjusted until the simulated brightness temperatures at the three channels match closely with the AMSR-E observed brightness temperatures at the same location (Njoku *et al.* 2003). The algorithm derived VegWC, soil moisture and Ts global daily data is stored at the National Snow and Ice Data Center (NSIDC) website (<http://www.nsidc.org/data/amsre>). We acquired VegWC data from this web site for our study regions and the time period of interest.

NDVI is a biophysical parameter that quantifies the photosynthetic activity of vegetation by observing the

“greenness” of the vegetation which is related to the chlorophyll abundance and energy absorption (Myneni *et al.* 1995; Tucker 1979). NDVI has been widely used for various studies on dynamic land surface changes such as deforestation and drought and as an important variable to model simulations such as land surface hydrology and land-atmosphere interactions.

NDVI is derived using the normalized ratio of the red and near-infrared surface reflectances (Tucker 1979). MODIS also provides surface temperature (Ts), which is derived from thermal infrared data (Wan & Li 1997; Justice *et al.* 1998). Surface temperature is an important variable linking evapotranspiration (ET) to soil moisture availability. Lower soil moisture and ET yield higher surface temperature and greater sensible heating of the atmosphere (Small & Kurc 2003). We used day values (1030AM equatorial overpass) from the daily 1 km resolution Ts data of MODIS. LAI is defined as the one-sided green leaf area per unit ground area in broadleaf canopies and as the projected needle leaf area in coniferous canopies (Myneni *et al.* 2002). LAI affects the fluxes of energy, mass, and momentum between the surface and the planetary boundary layer (Justice *et al.* 1998). The MODIS LAI is derived from a vegetation land cover classification and MODIS surface reflectance (Myneni *et al.* 1997; Justice *et al.* 1998). The algorithm uses six biome types which represent architecture of an individual tree and transmittance of vegetation elements.

From AMSR-E, VegWC is retrieved from a radiative transfer model in which vegetation opacity is used to derive VegWC at low frequency (Njoku & Li 1999). The AMSR-E VegWC possibly has biased data values particularly on water bodies and bare soil areas. AMSR-E VegWC is derived from surface roughness parameter incorporating effects both of vegetation and roughness (Njoku *et al.* 2003; Njoku & Chan 2005). Since roughness and vegetation have similar trends in their effects on the normalized polarization differences, the algorithm assumes the surface roughness parameter as VegWC (Njoku & Chan 2005). However, this assumption is acceptable only for smooth surface with vegetation. For example, a non-zero VegWC value in a desert area is only due to surface roughness. To avoid this error, we selected study regions primarily not including any water bodies and bare soil areas, and assumed that the selected regions have smooth vegetated surface and are not affected by any surface

roughness other than vegetation. In the case of irrigated/flooded land surfaces, the soil moisture retrieved from the AMSR-E brightness temperature will show saturated values but the retrieval of VegWC will be unaffected.

Additionally we created a new satellite variable using VegWC and LAI. Ceccato *et al.* (2001, 2002) found that NDVI and VegWC did not co-vary in a simple fashion, which may be attributed to differences between biomes in contrasting climatic regimes. A decrease in chlorophyll content, which is considered to reflect a decrease in NDVI, does not directly indicate a decrease in VegWC and vice versa. Larger vegetation structures are likely to have higher vegetation water content. In order to examine the indirect relationships between the variables, we made a new variable, the Normalized Vegetation Water Content (NVegWC) defined as VegWC per unit plant leaf area (the ratio of VegWC and LAI), which is linked with the leaf water conservation mechanism. It is a very useful descriptor especially when we compare vegetation across biomes which may have different species of vegetation with different leaf area indices and vegetation water contents. Our intent with calculating NVegWC was to facilitate a biome-to-biome comparison of vegetation water content and its relationship with other variables such as NDVI.

Data processing for satellite variable comparisons

All MODIS data sets used in this study have a 1 km spatial resolution while AMSR-E data is at 25 km with a different map projection type. Thus, in this study all data sets had to be resampled to be consistent with each other. All 1 km MODIS data were converted to 25 km resolution as AMSR-E data, and the different spatial projection types between MODIS and AMSR-E were changed to the same AMSR-E geographical projection. The sinusoidal projection of MODIS data sets was converted into the AMSR-E geographical projection by nearest neighbor method with the help of MODIS re-projection tool (developed by NASA), and 25 pixels of 1 km MODIS data were aggregated and averaged to compose the 25 km spatial resolution. Then each data set has been averaged for the three-month summer season (9 June to 12 September). When data sets are re-sampled, errors are inevitable. To minimize this error, we removed the cloud-contaminated MODIS data pixels based on the data retrieval

quality information provided for every pixel and then analyzed the standard deviation for each process. Linear and nonlinear regression analyses were conducted to find correlations between the variables, and one of the variables was color-coded into the two-variable relationship. The value of NVegWC was color-coded in the Ts-NDVI relationship.

Model description

We used the coupled Noah/WRF model for the model tests. This model was originally designed by Chen & Dudhia (2001) with the fifth-generation Mesoscale Model (MM5) and the Oregon State University land surface model (OSULSM or later Noah LSM). The MM5 model has been jointly developed by the Pennsylvania State University and the National Center for Atmospheric Research (NCAR). This model has been widely used for numerical weather prediction, air quality studies, and hydrological studies. The motivation of the coupling of the MM5 and the Noah LSM was the existing simple LSM in MM5 which was not compatible to the complexity of physical processes of land surface. The Weather Research and Forecasting (WRF) model, a successor of the MM5 with the model coupling technique, is a mesoscale model for numerical weather forecasting and data assimilation system (Skamarock *et al.* 2005). Maintained and supported as a community model to facilitate wide use for researching and teaching in the university community, the WRF model is suitable for use in a broad spectrum of applications across scales ranging from meters to thousands of kilometers. This includes research and operational numerical weather prediction, data assimilation, and parameterized-physics research, downscaling climate simulations, driving air quality models, and etc, and also offers numerous physics options such as microphysics, surface physics, atmospheric radiation physics, and planetary boundary layer physics.

The Noah LSM used for this model-coupling approach was originally developed by Pan & Mahrt (1987). Its hydrological physics is based on the diurnally dependent Penman potential evaporation approach (Mahrt & Ek 1984), the multilayer soil model (Mahrt & Pan 1984), and the primitive canopy model (Pan & Mahrt 1987). This model has been extended with a canopy resistance formulation and a surface runoff scheme by Chen *et al.* (1996) and implemented into the

MM5 and WRF model for the model coupling system. In the Noah LSM of the coupled model, ET is expressed as the sum of direct evaporation from ground and canopy surface and transpiration through vegetation (Chen & Dudhia 2001). Direct ground evaporation (EDIR) is estimated from a simple linear method (Betts *et al.* 1997), and canopy surface evaporation (EC) is calculated from similar methods of Noilhan & Planton (1989) and Jacquemin & Noilhan (1990). Vegetation transpiration (ETT) is very similar to the EC formulation, but canopy resistance is included in its calculation. The canopy resistance which has been extended by Chen *et al.* (1996) in the Noah LSM is estimated by the formulation of Jacquemin & Noilhan (1990), representing the effects of solar radiation, vapor pressure deficit, air temperature, and soil moisture. The main procedure of the estimation process of surface moisture flux in Noah LSM is as follows. Once obtaining initial land states, surface characteristics, and atmospheric forcing data, the model calculates land-atmospheric heat and moisture exchange coefficients with soil conductivity and diffusivity. Then, these coefficients are used to estimate potential evaporation which becomes the basis of the moisture flux estimation after combined with the canopy resistance.

The coupled WRF/Noah model has two major problems: (1) overestimation of latent heat flux (LH) probably induced by vegetation effects and (2) absence of routine soil moisture observations at regional and global scale for the model initial condition. In the previous study (Hong *et al.* 2009), even though proper soil moisture initialization from field observation data for several locations resulted in reasonable simulations of soil moisture variations, LH simulations responded very sensitively to those variations, showing overestimations when soil moisture and vegetation amount were relatively high. In the Noah LSM, the vegetation fraction (Fg), which is defined as area ratio of vegetation and defined area such as a pixel, plays a very important role in the determination of the each component of ET. However, the Fg parameter used in the current LSM came from 5-yr monthly Advanced Very High Resolution Radiometer (AVHRR) data (1986–91) with 0.15° spatial resolution which is about 15 km in Central America (Gutman & Ignatov 1998). Considering that one of the merits of the recently advanced WRF model is to provide simulations with very high resolution of 1 km or even higher, the Fg parameter in the coarser resolution may increase the model accuracy to the same degree if we had fine scale

vegetation data. In terms of temporal resolution, monthly Fg data cannot provide enough information to describe short-term variations of land cover such as in weekly or bi-weekly periods (Hong *et al.* 2007). Anthropogenic activities such as crop harvest may cause a big change of land cover in just a few weeks. Moreover, the interannually invariant Fg parameter is not congruous to annual land cover changes. Thus, Fg needs to be parameterized with more compatible temporal and spatial resolution for improved model simulations.

Absence of routine soil moisture measurement data at regional and global scale is obviously followed by low reliability of the model simulations. There are currently available input sources for usage of the model initialization such as National Center for Environmental Prediction (NCEP) final analysis data with 1 degree and 6 hour resolution, NCEP/NCAR Reanalysis data with 2.5 degree and 6 hour resolution, NCEP GRIB Global Data Assimilation System (GDAS) with 2.5 degree and 12 hour resolution, and NCEP regional operational Eta with 40 km and 6 hour resolution. When the coupled MM5/Noah model was designed by Chen & Dudhia (2001), the Eta model simulation data were selected for the model initialization due to their relatively high spatial resolution for initial land states, large spatial coverage over North American area, and similar physics of atmospheric forcing as used in Noah LSM. For the same reason as for the Fg parameter above, the 40 km resolution of Eta model is not compatible with finer model simulations, for example, with the 1 km resolution which is used in this study. Coarse resolutions of initial data are generally followed by more interpolations to produce finer resolution outputs in the model. The difference in spatial resolution causes model biases.

Ground observation data and model configuration over the IHOP_2002 area

The main goal of IHOP_2002 is to obtain accurate and reliable measurements of near-surface moisture status which is very important for meteorological parameterization 2002 (Weckwerth *et al.* 2004). These observations were carried out during a growing season from May to June 2002 with various field facilities. During the IHOP_2002 period, NCAR and University of Colorado installed surface flux stations, called Integrated Surface Flux Facilities (ISFF), to

support the IHOP_2002 atmospheric boundary mission in Southern Great Plains (Chen *et al.* 2003). The 9 ISFFs installed by NCAR, which were located in between Eastern Kansas and the Oklahoma Panhandle, are categorized as western (sites 1, 2, and 3), central (sites 4, 5, and 6), and eastern (sites 7, 8, and 9) tracks (Figure 2). The stations along the western track are located in south to north of the Oklahoma panhandle, and the ones along the central and eastern track are aligned west to east in southwest of Wichita, Kansas. The area around the each station track shows characteristic surface condition related to soil moisture and vegetation cover. Along the western track, MODIS NDVI was between 0.1 and 0.4, and soil moisture at 5 cm depth was less than $0.1 \text{ m}^3 \text{ m}^{-3}$ in a dry period from 20 May to 27 May 2002. On the other hand, the eastern area including the eastern ISFF stations showed relatively high soil moisture with over $0.3 \text{ m}^3 \text{ m}^{-3}$ on average and high NDVIs between 0.5 and 0.9. To summarize, the eastern area has more vegetation and cooler surface than does the western area (LeMone *et al.* 2007).

The domain configuration was set up to cover all NCAR ISFF stations with 1 km resolution (Figure 2). We set three nesting domains with 5:1 spatial ratio. From the set of the subject domain (Domain 3) over IHOP_2002 area with 1 km resolution, an outer domain (Domain 2) was set with 5 km, and then the mother domain (Domain 1) was set to cover about half of North America with 25 km resolution. Such domain configuration is controlled by a domain nesting system which allows us to increase the model spatial resolution by the mesh refinement method (Michalakes 2000).

Through this domain nest setting, smaller domains with higher resolutions take and/or give information about boundary conditions from bigger domains with lower resolutions. The covering area of each domain comprises 75 by 55, 206 by 106, and 526 by 186 grid boxes for domains 1, 2, and 3, respectively, and each grid box represents a square area with the given length from the resolutions (25 by 25, 5 by 5, and 1 by 1 km, respectively).

Based on the soil moisture time series obtained from the field measurements, we set three simulating time configurations which are expected to represent the temporal heterogeneity of surface moisture status. According to the ISFF observations, each station showed a relatively dry period until a rainfall event on between 24 and 27 May 2002, and then the relatively high surface moisture condition gradually decreased until the next rainfall event around 4 June 2002. We set the high moisture period of the surface on between 24 and 27 May as WET period, and then the dry period before the WET as DRY1, and the one after the WET as DRY2. With this setting, we expected the sensitivity of the model response to the variation of the surface moisture condition when it goes from dry to wet period or vice versa. We set the model spin-up time for each period with 48 hours: from 22 May 00:00 to 24 May 00:00 for DRY1, from 28 May 00:00 to 30 May 00:00 for WET, and from 2 June 12:00 to 4 June 12:00 for DRY2.

Model parameterization and initialization

We tested the model sensitivities to changes of vegetation parameter and soil moisture initial condition through

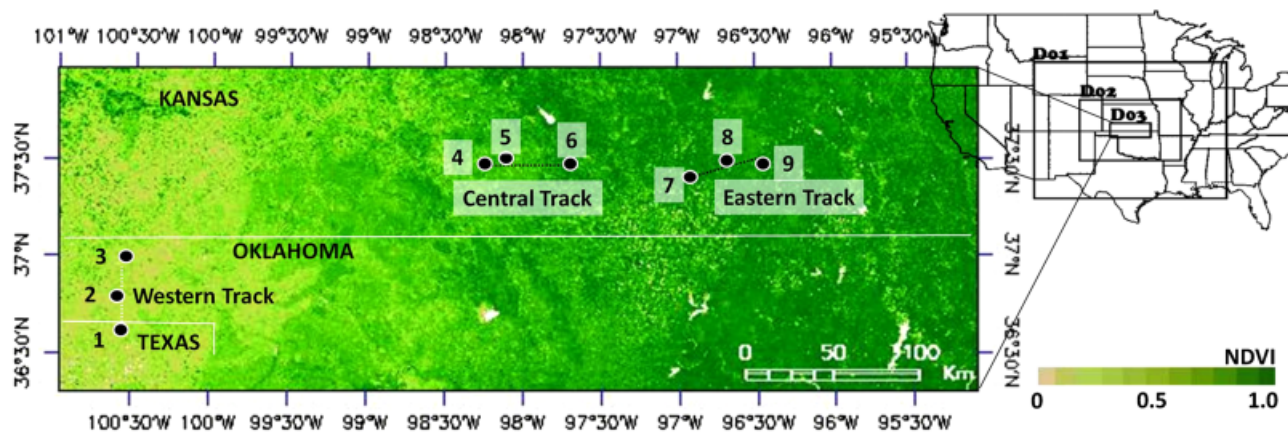


Figure 2 | Image of the study area with MODIS NDVI distribution over the IHOP_2002 study region and the model domain configuration scheme; dots in the image indicate the locations of the nine ISFF stations.

vegetation fraction (Fg) parameterization and soil moisture initialization. There are two popular methods for deriving Fg. One is used in the current coupled WRF/Noah model and derived by the following linear method (Gutman & Ignatov 1998):

$$Fg = \frac{NDVI - NDVI_{min}}{NDVI_{max} - NDVI_{min}} \quad (1)$$

where $NDVI_{min}$ is minimum NDVI (or bare soil NDVI) and $NDVI_{max}$ is maximum NDVI (or full canopy NDVI). The current model uses 0.04 for $NDVI_{min}$ and 0.54 for $NDVI_{max}$ which have been selected as seasonally and geographically invariant constants (Gutman & Ignatov 1998), and the monthly Fg data using global 5-year AVHRR NDVI (1986 to 1991) have been applied to the model Fg parameter. The other popular method to compute Fg is the quadric model (Carlson & Ripley 1997):

$$Fg = \left(\frac{NDVI - NDVI_{min}}{NDVI_{max} - NDVI_{min}} \right)^2 \quad (2)$$

Montandon & Small (2008) pointed out that underestimation of $NDVI_{min}$ causes overestimation of Fg, especially in a sparse vegetation area such as grassland in the western area, and this overestimation is minimized when using the quadric Fg method.

Considering the relatively high spatial and temporal resolution for new Fg parameters, we produced Fg from the MODIS data as mentioned above. There are two different MODIS platforms: Terra and Aqua, but we only used data from Terra MODIS due to data availability in 2002. To derive NDVI, we obtained 8-day 500 m surface reflectance from MODIS via <http://lpdaac.usgs.gov>, and NDVI is calculated as follows:

$$NDVI = \frac{NIR - R}{NIR + R} \quad (3)$$

where R is red infrared reflectance and NIR is near infrared reflectance. Those reflectances correspond to the MODIS sensor band 1 (620–670 nm) and band 2 (841–876 nm), respectively. Even though MODIS provides daily surface reflectance which may be able to offer vegetation variation on a daily basis, the data are not usable for this study due to data loss caused by cloud effects. Most recent studies have used 16-day MODIS NDVI imagery for deriving Fg (e.g., Miller *et al.* 2006; Montandon & Small 2008), but we selected 8-day MODIS reflectance to approach closely to the temporal resolution configured in this study. The MODIS data sets were spatially resized from 500 m to 1 km, 5 km, and 25 km resolutions through data aggregation for domains 1, 2, and 3, respectively. Then bad data pixels, contaminated by cloud effects, were eliminated and replaced by a null value. The applied MODIS data sets to the Fg parameterizations are 8-day 17 May 2002 data granules for DRY1 and 8-day 25 May 2002 data granules for WET and DRY2.

For the determination of $NDVI_{min}$ and $NDVI_{max}$, we used two different methods. One is to select them as invariant constant values among the local MODIS NDVIs in our study area (domain 3). In our case, the selected NDVI values were 0.04 and 0.80 for $NDVI_{min}$ and $NDVI_{max}$, respectively. The other method used in this study is to use a constant $NDVI_{min}$ but variant $NDVI_{max}$. In the physics of canopy resistance applied to the Noah LSM, vegetation parameters such as maximum/minimum stomatal resistance, leaf area index, and leaf cuticular resistance have constant values for each land cover type. Thus, it is likely to be beneficial to obtain better LH simulation if Fg derivation is associated with land cover types. In this study, we adopted a constant $NDVI_{min}$ (0.07) and variant $NDVI_{max}$ which were derived using Zeng *et al.*'s (2000) method for 2003 MODIS NDVI data as in the study of Montandon & Small (2008). Table 1 summarizes the methods used for the Fg parameterizations in this study. We named each method as BASE, VEG1, and VEG2 as shown in Table 1.

Table 1 | Summary of the coupled model simulations

CASE	BASE	VEG1	VEG2	HRLDAS
Fg Parameter	Monthly AVHRR Linear	8 day MODIS Linear	8 day MODIS Quadric	8 day MODIS Quadric
Soil Moisture Initial condition	40 km NCEP Eta	40 km NCEP Eta	40 km NCEP Eta	1 km HRLDAS

In order to provide improved land-state initialization for the coupled WRF/Noah model, HRLDAS (High Resolution Land Data Assimilation System is an offline, uncoupled land surface model into which all surface data sets are assimilated. HRLDAS provides the best surface fields for WRF initialization) is being developed at NCAR and executed in uncoupled mode of the Noah LSM by interpolating land surface variables from observed atmospheric forcing conditions (Chen et al. 2007). An advantage of HRLDAS is the consistency with the coupled WRF/Noah model system because it uses the same WRF nested grid configuration such as resolution, grid points, and projection and the same land surface parameters such as land use, soil texture, terrain height, and vegetation properties. HRLDAS reads those sources from WRF input files generated by WRF Standard Initialization (SI) or WRF Preprocessing System (WPS). Atmospheric forcing data used on HRLDAS includes hourly 4-km NCEP stage-IV rainfall analyses data (Fulton et al. 1998), hourly 0.5-degree downward solar radiation derived from the Geostationary Operational Environmental Satellite (GOES) (Pinker et al. 2003), and three-hourly atmospheric analyses from NCEP Eta Data Assimilation System (EDAS) (Rogers et al. 1995). With the model basis of Noah LSM, HRLDAS uses four soil layers to present daily, weekly, and seasonal soil moisture variation.

In this study, we produced input files for HRLDAS using WRF SI. Chen et al. (2007) experimented HRLDAS spin-up dependency to find out its equilibrium state for various soil layers and pointed out that fine soil texture with low hydraulic conductivity requires longer spin-up time to reach the equilibrium state. Based on their study we ran HRLDAS for about 13 months which is a typical runtime span for most soil

types for their equilibrium, starting from April 2001. The soil moisture generated by HRLDAS was used for the model initial conditions, combined with the quadric Fg model parameterization method.

RESULT

Satellite data comparisons

We investigated how surface temperature varies with NDVI and VegWC. Figure 3 (seasonal means for different pixels) shows (a) General description about the relationship between T_s and NDVI (or vegetation greenness) and (b) the relationship diagrams for the study regions. This relationship, termed as the TvX relationship, has been examined in many previous studies as a fundamental descriptor of the land surface state related with surface moisture availability and hence ET (Nemani & Running 1989, Sandholt et al. 2002). The geometry of the TvX relationship shows regional, climatic and biome dependence (Goetz 1997; Sandholt et al. 2002), and our study regions fall within the triangle-shaped geometry, showing a good contrast of general climatic and vegetation characteristics in each study region. The clustering of the points from each of the three regions on the TvX plot shows the importance of climate and vegetation characteristics. The TvX relationship of the NAMS region in the figure is distributed in the range of upper and left area, which indicates very low vegetation and dry condition with high potential evaporation. The IHOP region in this relationship shows relatively wetter climate than the NAMS region with more partial canopy. Tifton, GA, on the other hand, shows fuller vegetation and

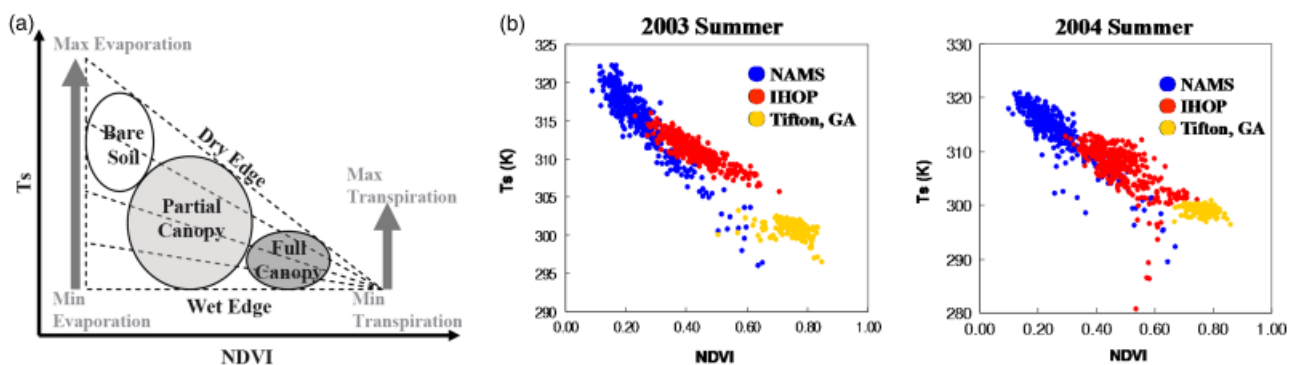


Figure 3 | (a) A schematic TVX relationship and (b) regional TVX distributions of three regions.

very wet climate with high potential transpiration. With low evaporation, T_s of bare soil is much higher than that of plant canopies, and therefore a negative slope exists along the dry or warm edge. This slope in the T_s - X relationship is steeper in dryer conditions (Goetz 1997; Nemani *et al.* 1993). In Figure 4, the steepness of the negative slopes is higher in the NAMS region. Through the regression analyses of the T_s - X relationship, the statistical correlation in the NAMS region is much stronger, compared with Tifton, GA. NVegWC has been color-coded into this T_s - X relationship in Figure 4, showing high NVegWC distributed in higher T_s and lower NDVI areas.

Figure 5 shows the NVegWC variation range for each land cover type. Even in the same vegetation type, NVegWC variations are different in each region, and the average values in the NAMS region are generally higher with wider variation range while Tifton, GA shows much less variation of

NVegWC with lower average values than the other regions. The major types of vegetation in the NAMS region (shrublands and savannas) show relatively high NVegWC with very high variation. Thus, the result in Figure 3 can be explained as the tendency of vegetation behavior, which is high water-leaf vegetation with low NDVI indicating more water exists in vegetation leaves of more arid environments. Arid regions with low NDVI, however, do not have a continuous canopy cover but a sparse coverage...for example, clumps of vegetation interspersed with bare soil area. Since the T_s of bare soils is always larger, for daytime measurements, than that of transpiring vegetation in summer season, the T_s of the NAMS region is higher than that of the other two regions considered in this study (Figures 3 and 4). Because of this influence of discontinuous vegetation coverage on T_s , the relationship between NVegWC and T_s in such arid areas can be overstated, but the NVegWC-NDVI relation

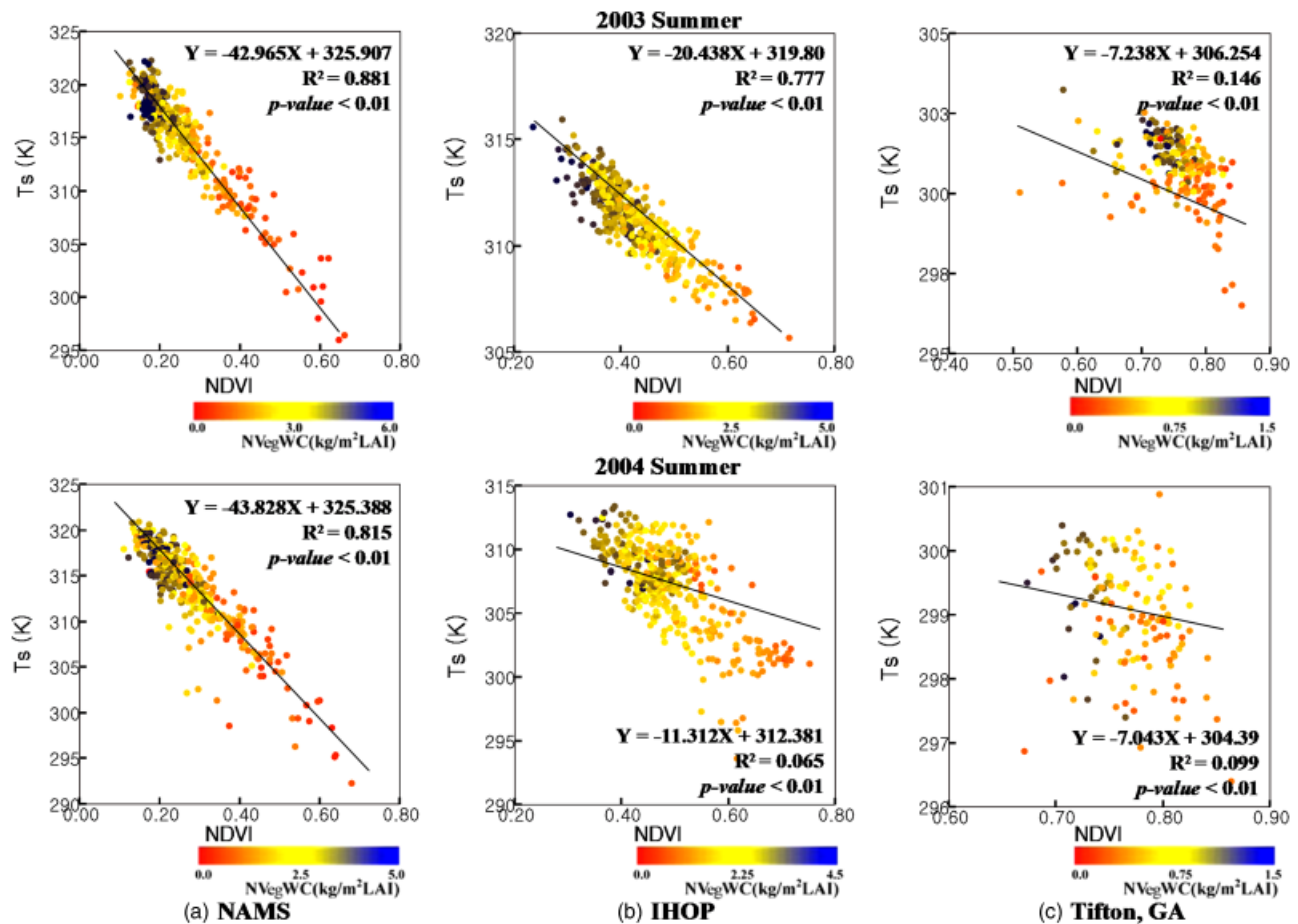


Figure 4 | The regression analysis of the TVX relationships color-coded with NVegWC: (a) the NAMS region, (b) the IHOP region, and (c) Tifton, GA.

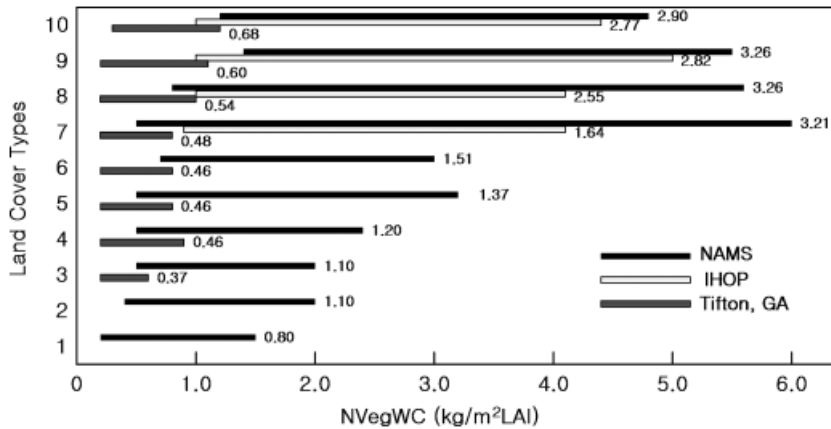


Figure 5 | NVegWC variation in different land cover types for summer season of 2003 and 2004 (the numbers of land cover types follow the IGBP classification). The denoted numbers are the NVegWC average values for each range bar. IGBP land cover units: 1. Evergreen needleleaf forests >60% cover, height exceeding 2 m, green all year; 2. Evergreen broadleaf forests >60% cover, height exceeding 2 m, green all year; 3. Deciduous needleleaf forests >60% cover, height exceeding 2 m, annual leaf on/off cycle; 4. Deciduous broadleaf forests >60% cover, height exceeding 2 m, annual leaf on/off cycle; 5. Mixed forests >60% cover, height exceeding 2 m, mixed four forest types; 6. Closed shrublands >60% cover, less than 2 m tall, evergreen or deciduous; 7. Open shrublands 100% cover, less than 2 m tall, evergreen or deciduous; 8. Woody savannas 30-60% cover, height exceeding 2 m, evergreen or deciduous; 9. Savannas 10-30% cover, height exceeding 2 m, evergreen or deciduous 10. Grasslands <10% cover.

provides enough evidence for the conclusions reached in this study.

Coupled model tests

Figure 6 shows the temporal variations of simulated land surface variables, and Table 2 provides their statistical comparisons to the ISFF observations with correlation coefficients (R-square values from regression analyses) and root mean square errors (RMSE). Relatively low correlations were observed in GH and LH in the eastern area while the other areas showed good correlations with the observations. The comparisons of their temporal variations and RMSE make possible various interpretations.

In order to test only vegetation effect by F_g parameterization, soil moisture initial values for the nine ISFF station sites were replaced by the observed data. With this data replacement for the soil moisture initial condition, low atmospheric variation in each simulation period resulted reasonable soil moisture simulations in the coupled WRF/Noah model; there was no observation of any substantial rainfall during each period, except from 5 to 20 mm of precipitation at the end of DRY1. Generally the soil moisture initial conditions were adjusted to be lowered in the western and central areas and to be raised in the eastern area.

The effects of F_g parameter on surface temperature (T_s) simulation were observed mainly during DRY2 in the eastern

area, showing about 5 K decrease of the diurnal peaks, while those of the other regions showed slight or no improvement. RMSE of T_s simulations, however, did not show any significant difference among the cases. The average RMSE of T_s simulations were about 3 K. The T_s underestimation in the eastern area is the locations where soil moisture was around $0.38 \text{ m}^3 \text{ m}^{-3}$, but this does not indicate soil moisture effect from the data replacement but rather the vegetation effect from the F_g parameterizations. Increase in F_g amount caused lowered the T_s . This is also supported by the HRLDAS test as described in the next section.

While T_s underestimations were observed, sensible heat (SH) simulations showed significant improvement during especially WET and DRY2 in the eastern area. The SH simulations agree very closely with the observations with about 200 Wm^{-2} decrease during DRY2 in that region. RMSE of SH also supports this improvement that was observed in both of the F_g parameterizations. In the eastern area, RMSE of SH improved from 91.07 Wm^{-2} to about 40 Wm^{-2} . SH values of the diurnal peaks in that region decreased by 100 Wm^{-2} during DRY1, 120 Wm^{-2} during WET, and 200 Wm^{-2} during DRY2 which are very close values to the SH observations. No substantial difference between VEG1 and VEG2 was observed because F_g parameters were very similar in the eastern stations. On the other hand, SH during DRY2 in the central track showed overestimations and increased by 100 Wm^{-2} from that of the

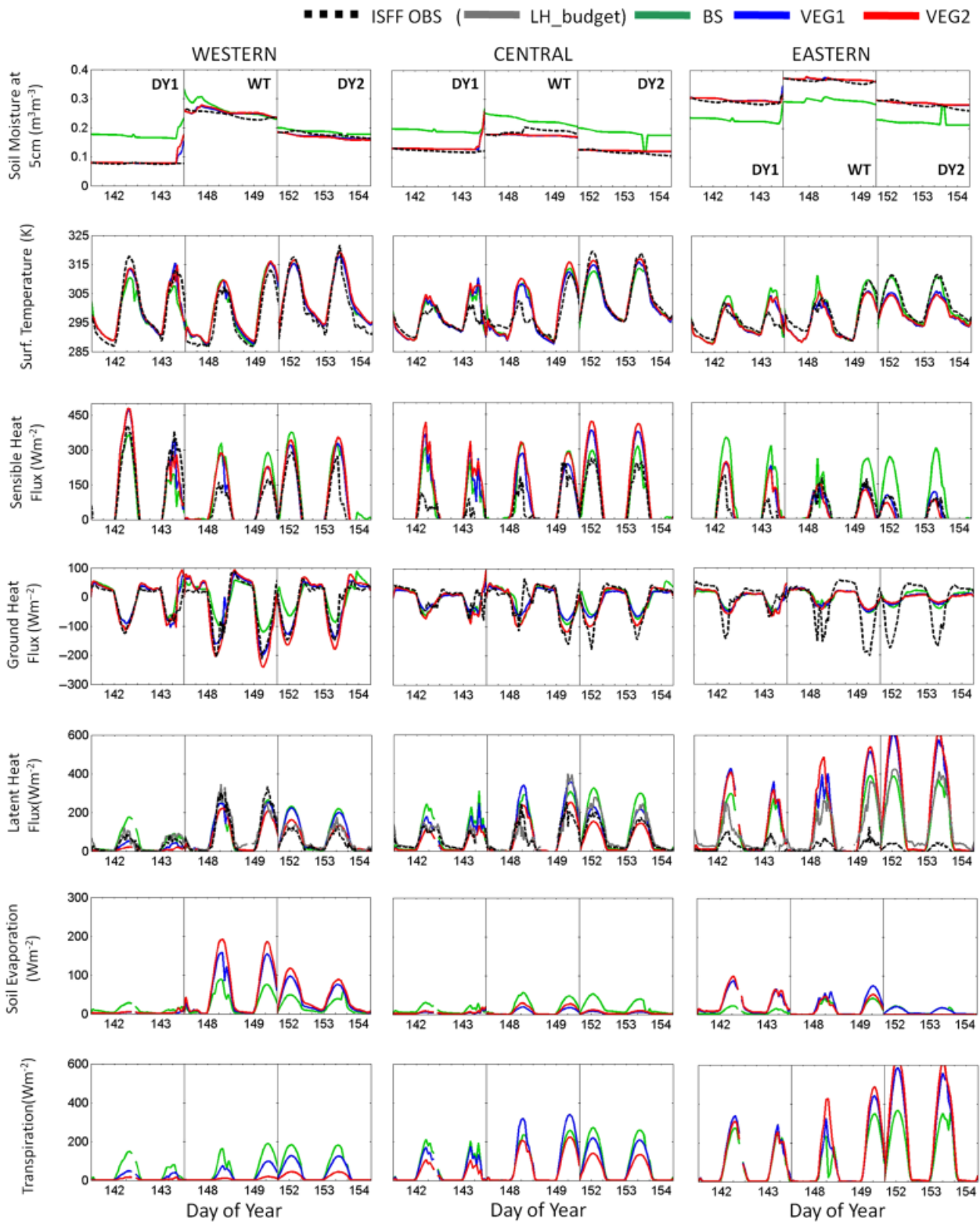


Figure 6 | Temporal variations of land surface variables simulated by the WRF/Noah model and their comparisons to the ISFF observations for the BASE, VEG1, and VEG2 cases.

Table 2 | Correlation coefficients and RMSE of simulated land surface variables to ISFF observations

		Western		Central		Eastern	
		R ²	RMSE	R ²	RMSE	R ²	RMSE
T _S (K)	BASE	0.86	3.71	0.78	3.57	0.82	2.91
	VEG1	0.92	3.09	0.81	3.41	0.82	2.98
	VEG2	0.91	3.47	0.79	3.95	0.78	3.30
	HRLDAS	0.92	3.83	0.80	4.01	0.79	2.90
SH (Wm ⁻²)	BASE	0.67	78.28	0.68	76.35	0.62	91.07
	VEG1	0.81	62.60	0.75	85.90	0.73	38.33
	VEG2	0.78	70.16	0.73	106.55	0.69	40.74
	HRLDAS	0.86	68.53	0.80	102.86	0.67	63.85
GH (Wm ⁻²)	BASE	0.80	36.56	0.60	33.37	0.66	51.25
	VEG1	0.89	24.23	0.72	30.02	0.62	52.03
	VEG2	0.89	33.53	0.74	27.38	0.50	54.09
	HRLDAS	0.89	42.72	0.73	28.39	0.50	54.47
LH (Wm ⁻²)	BASE	0.72	47.51	0.81	69.57	0.58	151.52
	VEG1	0.76	39.66	0.80	58.57	0.56	218.63
	VEG2	0.83	33.14	0.75	37.03	0.53	234.86
	HRLDAS	0.94	39.64	0.77	34.99	0.49	188.61
LH_Budget (Wm ⁻²)	BASE	0.74	46.70	0.73	63.67	0.81	61.94
	VEG1	0.79	40.72	0.70	59.03	0.87	100.80
	VEG2	0.83	38.05	0.66	57.92	0.87	114.43
	HRLDAS	0.90	44.91	0.70	60.53	0.91	69.46

BASE case. RMSEs also increased by 30 Wm⁻² in the VEG2 case. The other periods (DRY1 and WET) in the central area showed no significant changes in SH simulations. Meanwhile, in the western area, less influence of Fg parameter was observed, and SH overestimation during DRY1 of the VEG1 and VEG2 cases is interpreted as the model high sensitivity to soil moisture variation in that region.

Ground heat flux (GH) simulations did not show any vegetation effect in the high vegetated areas, showing low correlations and hence low reliability in the GH simulations of the model. The low diurnal variations of simulated GH in the eastern area were not improved either by the Fg parameterizations or soil moisture initialization. GH RMSEs in this region showed over 50 Wm⁻² which is more about 20 Wm⁻² than those of the other regions. Considered that the range of the GH diurnal cycle (from about 80 Wm⁻² to 200 Wm⁻²), this error is quite significant. The greatest difference between the observations and the simulations were up to 150 Wm⁻². On the other hand, some simulation improvements especially

in the VEG1 case were observed during WET and DRY2 in the low vegetated region (the western area).

Latent heat (LH) simulations were very sensitive to Fg in highly vegetated area. The stations in the eastern track were contaminated, so we used the radiation budget method for the LH calculation with measured net radiation (R), SH, and GH in this study, naming it “LH_budget”. The correlations of LH simulations with the observations have been substantially improved when it was compared with the LH_Budget data set. Noticeable LH overestimations in that area were observed and the differences from the LH_budget observation were as much as 200 Wm⁻². This LH overestimation was also reported in the studies of [Chen *et al.* \(2007\)](#) and [Hong *et al.* \(2009\)](#), which used the same Noah LSM implemented into HRLDAS and into the WRF model, respectively. Any substantial difference between the VEG1 and VEG2 cases was not observed in the eastern region, but the central (in all periods) and western areas (during DRY2) show improved simulations in the VEG2

case. The error statistics through RMSEs of LH also demonstrates this phenomenon; RMSE were observed to be better in VEG1 (about 6 Wm^{-2} and 3.5 Wm^{-2} improvements in the western and central area, respectively) and VEG2 (about 7.5 Wm^{-2} and 6 Wm^{-2} improvements in the western and central area, respectively) cases in relatively low vegetated area but worse in the eastern area (about 39 Wm^{-2} and 52 Wm^{-2} worse in VEG1 and VEG2 cases, respectively) as verified with LH_budget observations. When compared with LH observations, the central area shows better results with a lower RMSE (about 39 Wm^{-2} improvement in the VEG2 case). The analyses of the temporal variations of the ET components, EDIR and ETT, were performed in order to understand the LH overestimations in the eastern area. EC generally occurs in a very short time, taking a very small portion of the total ET after precipitation. Since the model was configured to avoid any precipitation for clear sky conditions during the spin-up periods, we omitted analyzing EC in this result section. EC was a very small portion in our model simulations (less than 10 Wm^{-2} on average) and can be ignored for LH analyses. According to the result, the LH overestimation is mainly due to the overestimation of vegetation transpiration. LHs were overestimated in both VEG1 and VEG2 cases with about 250 Wm^{-2} more than those of the BASE case. Hong *et al.* (2009) have more emphasized the soil moisture effect for these LH overestimations, but our study provides a different point of view. With the HRLDAS case study, we present that the vegetation effect is more responsible for the LH overestimation than soil moisture variation.

Figure 7 shows the temporal variation of the surface variables simulated by the coupled WRF/Noah model, and Table 2 also provides the statistical analyses for this HRLDAS case. Briefly, relatively good correlations with observations were observed in most variables except GH and LH in the eastern area similarly as in Fg cases; R^2 was 0.5 for GH. The low coefficient of LH simulations was improved when it was compared to LH_budget (from 0.49 to 0.91). Soil moistures simulated by HRLDAS were improved in the western and central regions but showed almost no change in the eastern area. This soil moisture improvement, however, did not have a significant effect on T_s simulations, but the vegetation does have an impact and displays a very similar pattern of the T_s diurnal cycle as that in VEG2 cases. Moreover, the T_s underestimations in the eastern area support the Fg effect as

discussed in the previous section. Meanwhile, the second T_s peak values in the western area give us an interesting implication about the model. In the soil moisture variations of the VEG2 and HRLDAS cases, HRLDAS showed higher soil moisture ($0.13 \text{ m}^3 \text{ m}^{-3}$) than that in VEG2 ($0.08 \text{ m}^3 \text{ m}^{-3}$), but the second T_s peak value during DRY1 was higher in HRLDAS (319 K) than that in VEG2 (315 K). This result of the T_s increase in spite of soil moisture increase in low vegetated area indicates a greater sensitivity of the model to Fg parameter but not to soil moisture even in such region (Fg was 0.09 in the western station sites of VEG2 in average).

Unlike the improved SH simulations in the VEG1 and VEG2 cases in the eastern track, the ones of HRLDAS did not resemble the observed diurnal cycle due to negligible soil moisture change in the region. This indicates that the SH simulation is affected not only by vegetation but also by soil moisture variation. While the central area showed similar results as in the VEG2 case, the western area indicated the model sensitivity to soil moisture variation as discussed in the previous section. During the WET period in the western area, soil moisture did not display any quantifiable variability in all cases in this study. This resulted in little change of SH simulations in that period, indicating low sensitivity to Fg parameter. On the other hand, while soil moisture was lowered to $0.1 \text{ m}^3 \text{ m}^{-3}$ during DRY1 in that region, SH of the VEG2 case increased by about 100 Wm^{-2} in the first peak time of that period. A similar result was observed in the HRLDAS case (SH increased by 50 Wm^{-2}), but the difference in the SH peak values between these two cases explains the SH overestimation to be caused by soil moisture variation in such low vegetated area.

GH in the coupled model is not sensitive to soil moisture variation, showing very similar results as the VEG1 and VEG2 cases, except relatively high fluctuations during DRY1 in the western area. This anomaly is assumed to be due to relatively high T_s simulation of the coupled model because GH estimation in the model physics is closely related to soil temperature which is regarded as T_s in very low vegetated regions.

LH overestimations by ETT overestimation were also observed in the eastern area in the HRLDAS case, indicating vegetation effect. From the HRLDAS case study, however, we found that the soil moisture variation was also effective in the ETT overestimation. Due to no soil moisture change in the

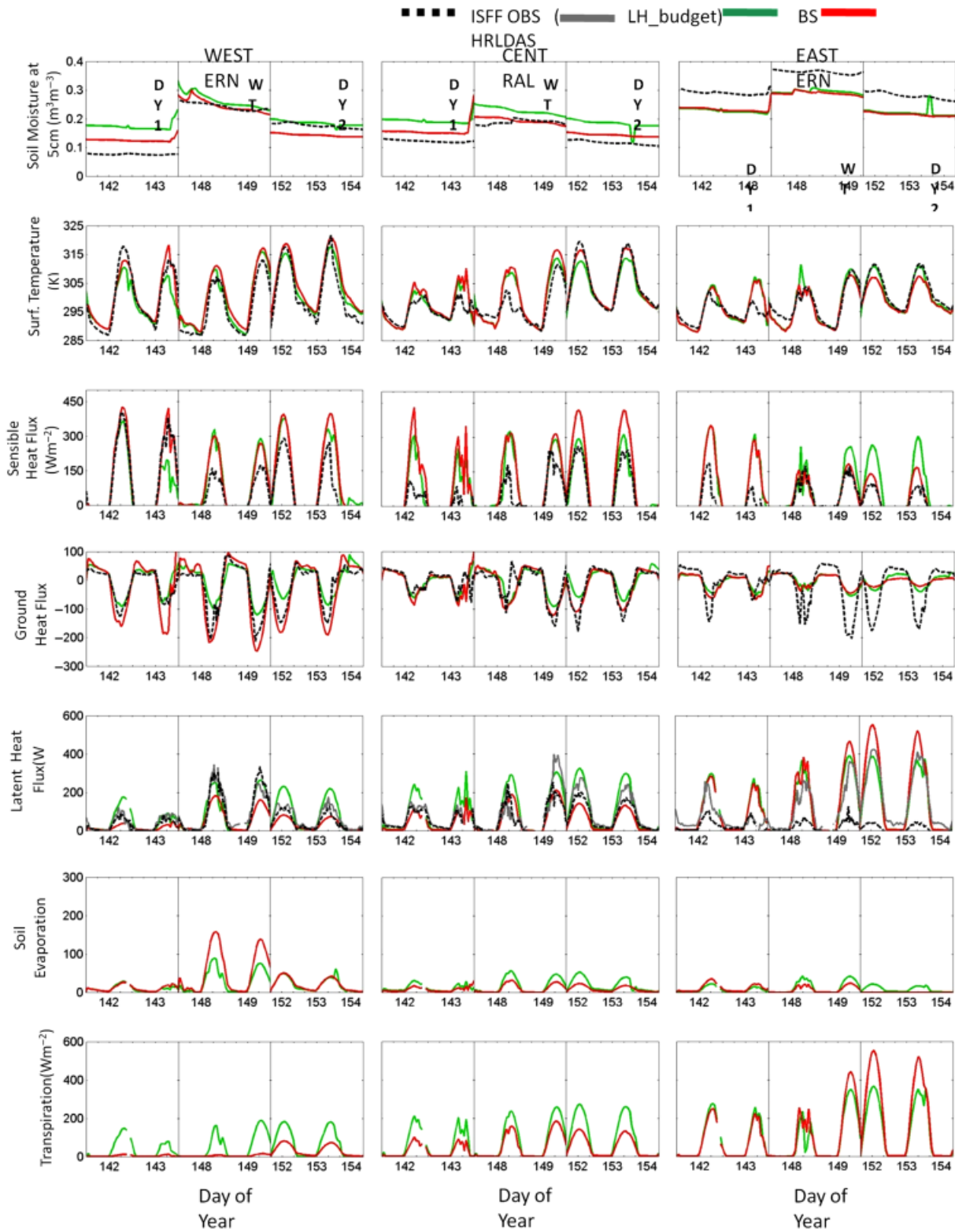


Figure 7 | Temporal variations of land surface variables simulated by the WRF/Noah model and their comparisons to the ISFF observations for the BASE and HRLDAS + VEG2 cases.

HRLDAS case, ETT showed less overestimation (up to 550 Wm^{-2}) than that in the VEG1 or VEG2 case (up to 630 Wm^{-2}). Thus, the ETT difference between the HRLDAS and VEG1 or VEG2 cases implies effect of soil moisture variation. In the western area, effects of both vegetation and soil moisture on ETT simulations were also observed; when Fg and soil moisture decreased during DRY1, ETT also decreased. EDIR simulations also support the dual effects; during WET in the western area, EDIR increased more up to about 200 Wm^{-2} by only Fg decrease than that by Fg and soil moisture decrease (up to about 160 Wm^{-2}). The RMSE of the LH simulations in the HRLDAS case showed significant improvement in the central area more than other cases (from comparisons with the LH observations). Meanwhile, they seem to show better result in the eastern area than that of the VEG1 or VEG2 case (from the statistics with the LH_budget), but this did not lead to any improvement from the BASE case (Table 2).

CONCLUSIONS

We have examined the inter-relationship between vegetation water content, vegetation and leaf area index and surface temperature in three contrasting hydroclimatic regions in the United States. The negative relationship between NVegWC and NDVI and between T_S and NDVI shows more water existence in plant leaves in more arid area, and the determination coefficients for those relationships of each region in the regression analyses explain the dependency of vegetation on water condition. It is generally assumed that the greenness of vegetation is related to photosynthesis which is dependent on solar radiation and the amount of carbon dioxide. Water content in vegetation is also utilized for the photosynthesis by which oxygen is released into the atmosphere, causing plant transpiration. Water amount in vegetation is more closely related to different vegetation types than to the greenness of vegetation which is considered as an indicator of photosynthesis. The photosynthesis process in vegetation is controlled under water stress condition indicated by precipitation, soil moisture and surface temperature. During the summer months, an increase in T_S implies an increase in water stress of vegetation, all other factors being equal, and moreover in arid regions T_S is more likely to impact water stress of vegetation than other factors. Vegetation physiologically responds to high water stress con-

dition by closing the stomata to control losing moisture and by having a deep and widely-spread root system to reach water sources in deeper soil (Cohen *et al.* 2005; Tanguiling *et al.* 1987). There are also some species, especially in arid area, that store more water in leaves during rainy season (Kramer 1983). Weighing the actual amount of water in different plant types separately for leaves, stems, and fruits/flowers, Sims & Gamon (2003) showed that in drought deciduous shrubs contain more water in their leaves than do evergreen tree leaves. These physiological responses of vegetation have been considered as adaptation mechanism to environment (Kramer 1983), and they would be more present in vegetation in arid regions where the water stress is a normal situation. Hence, the dominant vegetation in arid areas like the NAMS region is more likely to be adapted to their environment in a way to minimize their water loss than that in more humid area like Tifton, GA. In this study, LAI shows significant regional difference in values (NAMS: 0–2; IHOP: 0.5–2.5; Tifton, GA: 1.5–6), but the regional differences of VegWC values between the three regions is not as much (NAMS: 0–3 kg/m^2 ; IHOP: 1–4 kg/m^2 ; Tifton, GA: 1–4 kg/m^2). This can be explained as that the vegetation amount varies significantly under the regional climate condition, but the vegetation response shows a tendency to conserve water.

Through the model tests, the model sensitivity to vegetation and soil moisture variation was used to evaluate the model improvement from Fg parameterization and HRLDAS soil moisture initialization. The two Fg parameterization methods, the linear and quadric methods (VEG1 and VEG2) were used, and they resulted the better spatial west-east contrast of Fg distribution: less vegetation in the west and higher vegetation in the east. In many cases of this study, vegetation effects on the coupled model simulations by the Fg parameterization were observed either positively or negatively in terms of the model improvement. We obtained underestimation of T_S , overestimation of LH, and improvements of SH in highly vegetated region (the eastern area) and underestimation of GH in low vegetated region (the western area). According to the statistical analyses, we obtained improved results in SH simulations in the eastern area and in LH simulations in the western and central area for both VEG1 and VEG2 cases. Meanwhile, the HRLDAS case, combined with the VEG2 method, indicates both effects of vegetation and soil moisture variation. There was somewhat improvement from HRLDAS soil moisture initialization, but

this needs to be validated through further research with a longer period of simulation.

Among the various changes after the Fg parameterizations and/or HRLDAS soil moisture initialization, noticeable results were found as the low GH variability and LH overestimation in the eastern stations. According to the physics in the Noah LSM, soil temperature plays a key role in GH estimations, and soil temperature is function of soil moisture (Chen & Dudhia 2000). Thus, in the VEG1 or VEG2 case of the western area, lowered GH peak values during WET and DRY2 are due to soil temperature increase induced by Fg decrease from the newer Fg parameterizations. In the same view, the fact that high Fg amount in the eastern area (over 0.7 in all study cases) resulted in very low GH variability implies low soil temperature in that region, possibly by canopy shadow effect. With both results, this study indicates high sensitivity of GH simulation to Fg parameter. Nonetheless, the low GH variability from the model in the eastern area is still problematic, compared to GH observations. This may imply an excessive effect of vegetation.

On the other hand, LH simulations in the eastern area were also very sensitive to vegetation, showing overestimation of ETT. Finding the answer for the LH overestimation is quite challenging. The possible causes of LH overestimation

of the model can be considered as follows: (1) initial soil moisture changes, (2) overestimation of wind velocity, and (3) underestimation of air humidity at 2 m. The first case has been proved not to be very effective through this study. High wind intensity will be consequently followed by high ETT, but we could not observe any overestimation of wind from the model in the eastern area (Figure 8). Although the wind velocity of the east–west component during DRY2 in that area somewhat increased after the Fg parameterizations, its lower variation from the model was observed compared with the wind observations (Figure 8). The last case cannot be also counted because the Noah LSM uses air humidity just as a diagnostic variable. The Noah LSM uses the lowest model-level humidity (Ek & Mahrt 1991). Other possible answers about the ETT overestimations may be found in the relation with plant water stress and surrounding air condition such as CO₂ amount which affect the leaf stomata opening and closing which are the major factor to control vegetation transpiration (Betts et al. 1997; Hong et al. 2007).

This study has shown the impact of vegetation on the complex land and atmospheric interactions through the analyses of remote sensing data and through the coupled model tests. In particular, the model sensitivity tests to the vegetation variation indicate the need of more practical quantification or understanding of vegetation properties for more improved model simulations. These problems are related to the sensitivity to vegetation fraction presents mainly in vegetation transpiration, showing its overestimation. We have examined the proper representation of vegetation in a land–atmosphere model. Table 2 shows that even though we have good correlation (R values), the errors in flux estimates range from 30–80 W/m² which translates to between 5% and 30% of the flux estimation. This proves that for more accurate estimation of the fluxes we need better representation of vegetation in land models.

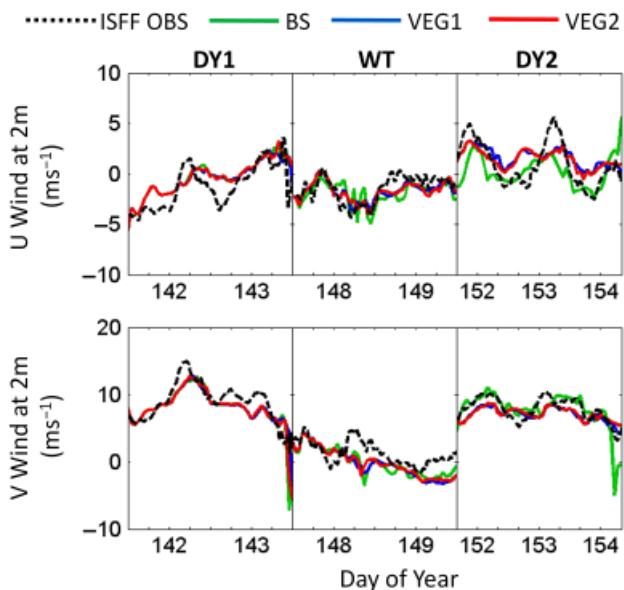


Figure 8 | Temporal variations of east–west (U) component (upper) and north–south (V) component (lower) wind velocity simulations and their comparison to the ISFF observations for the BASE, VEG1, and VEG2 cases in the eastern track.

REFERENCES

- Betts, R. A., Cox, P. M., Lee, S. E. & Woodward, F. I. 1997 *Contrasting physiological and structural vegetation feedbacks in climate change simulations*. *Nature* **387**, 796–799.
- Bosch, D. D., Davis, F. M. & Sheridan, J. M. 1999 *Rainfall characteristics and spatial correlation for the Georgia coastal plain*. *Trans. ASABE* **42**(6), 1637–1644.

- Carlson, T. N. & Ripley, D. A. 1997 On the relation between NDVI, fractional vegetation cover, and leaf area index. *Remote Sens. Environ.* **62**, 241–252.
- Ceccato, P., Flasse, S. & Gregorie, J. 2002 Designing a spectral index to estimate vegetation water content from remote sensing data (Part 2). *Remote Sens. Environ.* **82**, 198–207.
- Ceccato, P., Flasse, S., Tarantola, S., Jacquemoud, S. & Gregorie, J. 2001 Detecting vegetation leaf water content using reflectance in the optical domain. *Remote Sens. Environ.* **77**, 22–33.
- Chen, F. & Dudhia, J. 2001 Coupling an advanced land surface-hydrology model with the Penn State-NCAR MM5 modeling system. Part I: Model implementation and sensitivity. *Mon. Weather Rev.* **129**, 569–585.
- Chen, F., Manning, K. W., LeMone, M. A., Trier, S. B., Alfieri, J. G., Roberts, R., Tewari, M., Niyogi, D., Horst, T. W., Oncley, S. P., Basara, J. B. & Blanken, P. D. 2007 Description and evaluation of the characteristics of the NCAR High-Resolution Data Assimilation System. *J. Appl. Meteorol. Climatol.* **46**, 694–713.
- Chen, F., Mitchell, K., Schaake, J., Xue, Y., Pan, H., Koren, V., Duan, Q. Y., Ek, M. & Betts, A. 1996 Modeling of land surface evaporation by four schemes and comparison with FIFE observations. *J. Geophys. Res.* **101**(D3), 7251–7268.
- Chen, F., Yates, D. N., Nagai, H., LeMone, M., Ikeda, K. & Grossman, R. 2003 Land surface heterogeneity in the Cooperative Atmosphere Surface Exchange Study (CASES-97). Part I: Comparing modeled surface flux maps with surface-flux tower and aircraft measurements. *J. Hydrometeorol.* **4**, 196–218.
- Cohen, Y., Alchanatis, V., Meron, M., Saranga, Y. & Tsipris, J. 2005 Estimation of leaf water potential by thermal imagery and spatial analysis. *J. Exp. Bot.* **56**(417), 1843–1852.
- Ek, M. & Mahrt, L. 1991 *OSU 1-D PBL Model User's Guide. Version 1.04*, 120 pp. Available from Department of Atmospheric Sciences, Oregon State University, Corvallis, OR.
- Fulton, R. A., Breidenbach, J. P., Seo, D. J. S., Miller, D. A. & O'Bannon, T. 1998 The WSR-88D rainfall algorithm. *Weather Forecast.* **13**, 377–395.
- Goetz, S. J. 1997 Multi-sensor analysis of NDVI, surface temperature and biophysical variables at a mixed grassland site. *Int. J. Remote Sens.* **18**(1), 71–94.
- Gutman, G. & Ignatov, A. 1998 The derivation of the green vegetation fraction from NOAA/AVHRR data for use in numerical weather prediction models. *Int. J. Remote Sens.* **19**(8), 1533–1543.
- Hong, S., Lakshmi, V. & Small, E. E. 2007 Relationship between vegetation biophysical properties and surface temperature using multi-sensor satellite data. *J. Climate* **20**, 5593–5606.
- Hong, S., Lakshmi, V. & Small, E. E. 2009 Effects of vegetation and soil moisture on the simulated land surface processes from the coupled WRF/Noah model. *J. Hydrometeorol.* **114**, D18118, doi:10.1029/2008JD011249.
- Jacquemin, B. & Noilhan, J. 1990 Sensitivity study and validation of a land surface parameterization using the HAPEX-MOBILHY data set. *Boundary-Layer Meteorol.* **52**, 93–134.
- Justice, C. O., Vermote, E., Townshend, J. R., Defries, R., Roy, D. P., Hall, D. K., Salomonson V. V., Privette, J. L., Riggs, G., Strahler, A., Lucht, W., Myneni, R. B., Knyazikhin, Y., Running, S. W., Nemani, R. R., Wan, Z., Huete, A. R., Leeuwen, W. V., Wolfe, R. E., Giglio, L., Muller, J. P., Lewis, P. & Barnsley, M. J. 1998 The Moderate Resolution Imaging Spectroradiometer (MODIS): Land remote sensing for global change research. *IEEE Trans. Geosci. Remote Sens.* **36**(4), 1228–1249.
- Kleidon, A. & Heimann, M. 1998 Optimized rooting depth and its impacts on the simulated climate of an atmospheric general circulation model. *Geophys. Res. Lett.* **25**(3), 345–348.
- Kramer, P. J. 1983 *Water Relations of Plants*. Academic, New York.
- Kurc, S. & Small, E. E. 2004 Dynamics of evapotranspiration in semiarid grassland and shrubland during the summer monsoon season, central New Mexico. *Water Resour. Res.* **40**, W09305.
- LeMone, M. A., Chen, F., Alfieri, J. G., Tewari, M., Geerts, B., Miao, Q., Grossman, R. L. & Coulter, R. L. 2007 Influence of land cover and soil moisture on the horizontal distribution of sensible and latent heat flux in Southeast Kansas during IHOP_2002 and CASES-97. *J. Hydrometeorol.* **8**, 68–87.
- Mahrt, L. & Ek, K. 1984 The influence of atmospheric stability on potential evaporation. *J. Appl. Meteorol.* **23**, 222–234.
- Mahrt, L. & Pan, H. L. 1984 A two-layer model of soil hydrology. *Boundary Layer Meteorol.* **29**, 1–20.
- Michalakes, J. 2000 A parallel runtime system library for regional atmospheric models with nesting, in structural adaptive mesh refinement (SAMR) grid methods. In: *IMA Mathematics and Its Applications Series, Vol. 117*. Springer, New York, pp. 59–74.
- Miller, J., Barlage, M., Zen, X., Wei, H., Mitchell, K. & Tarpley, D. 2006 Sensitivity of the NCEP/Noah land surface model to the MODIS green vegetation fraction data set. *Geophys. Res. Lett.* **33**, L150404.
- Montandon, L. M. & Small, E. E. 2008 The impact of soil reflectance on the quantification of the green vegetation fraction from NDVI. *Remote Sens. Environ.* **112**, 1835–1845.
- Myneni, R. B., Hall, F. G., Sellers, P. J. & Marshak, A. L. 1995 The interpretation of spectral vegetation indexes. *IEEE Trans. Geosci. Remote Sens.* **33**(2), 481–486.
- Myneni, R. B., Hoffman, S., Knyazikhin, Y., Privette, J. L., Glassy, J., Tian, Y., Wang, Y., Song, X., Zhang, Y., Smith, G. R., Lotsch, A., Friedl, M., Morisette, J. T., Votava, P., Nemani, R. R. & Running, S. W. 2002 Global products of vegetation leaf area and fraction absorbed PAR from year one of MODIS data. *Remote Sens. Environ.* **83**, 214–231.
- Myneni, R. B., Ramakrishna, R., Nemani, R. & Running, S. 1997 Estimation of global leaf area index and absorbed PAR using radiative transfer models. *IEEE Trans. Geosci. Remote Sens.* **35**(6), 1380–1393.
- Nemani, R., Pierce, L., Running, S. & Goward, S. 1993 Developing satellite-derived estimates of surface moisture status. *J. Appl. Meteorol.* **32**, 548–557.
- Nemani, R. & Running, S. 1989 Estimation of regional surface resistance to evapotranspiration from NDVI and Thermal-IR AVHRR data. *J. Appl. Meteorol.* **28**, 276–284.
- Noilhan, J. & Planton, S. 1989 A simple parameterization of land surface processes for meteorological models. *Mon. Weather Rev.* **117**, 536–549.
- Njoku, E. G. & Chan, T. 2005 Vegetation and surface roughness effects on AMSR-E land observations. *Remote Sens. Environ.* **100**(2), 190–199.

- Njoku, E. G., Jackson, T., Lakshmi, V., Chan, T. & Nghiem, S. 2003 Soil moisture retrieval from AMSR-E. *IEEE Trans. Geoscience & Remote Sens.* **41**, 215–229.
- Njoku, E. G. & Li, L. 1999 Retrieval of land surface parameters using passive microwave measurements at 6–18 GHz. *IEEE Trans. Geosci. Remote Sens.* **37**(1), 79–93.
- Pan, H. L. & Mahrt, L. 1987 Interaction between soil hydrology and boundary-layer development. *Boundary-Layer Meteorol.* **38**, 185–202.
- Pielke, R. A. 2001 Influence of the spatial distribution of vegetation and soils on the prediction of cumulative rainfall. *Rev. Geophys.* **39**(2), 151–177.
- Pinker, R. T., Tarpley, J. D., Laszlo, I., Mitchell, K. E., Houser, P. R., Wood, E. F., Schaake, J. C., Robock, A., Lonmann, D., Cosgrove, B. A., Sheffield, J., Duan, Q., Luo, L. & Higgins, R. W. 2005 Surface radiation budgets in support of the GEWEX Continental Scale International Project (GCIP) and the GEWEX Americas Prediction Project (GAPP), including the North American Land Data Assimilation System (LDAS) Project. *J. Geophys. Res.* **108**, 8844.
- Rogers, E., Deaven, D. G. & DiMego, G. J. 1995 The regional analysis system for the operational “early” Eta model: Original 80-km configuration and recent changes. *Weather Forecast* **10**, 810–825.
- Sandholt, I., Rasmussen, K. & Andersen, J. 2002 A simple interpretation of the surface temperature/vegetation index space for assessment of surface moisture status. *Remote Sens. Environ.* **79**, 213–224.
- Shibata, A., Imaoka, K. & Koike, T. 2003 AMSR/AMSR-E level 2 and 3 algorithm developments and data validation plans of NASDA. *IEEE Trans. Geosci. Remote Sens.* **41**, 195–203.
- Sims, D. A. & Gamon, J. A. 2003 Estimation of vegetation water content and photosynthetic tissue area from spectral reflectance: a comparison of indices based on liquid water and chlorophyll absorption features. *Remote Sens. Environ.* **84**, 526–537.
- Skamarock, W. C., Klemp, J. B., Dudhia, J., Gill, D. O., Barker, D. M., Wang, W. & Powers, J. D. 2005 A description of the advanced research of WRF version 2. *Technical Report TN-468 + STR*, National Center for Atmospheric Research.
- Small, E. E. & Kurc, S. 2003 Tight coupling between soil moisture and the surface radiation budget in semiarid environments: Implications for land–atmosphere interactions. *Water Resour. Res.* **39**(10), 1278–1291.
- Tanguiling, V. C., Yambao, E. B., Toole, J. C. O. & De Datta, S. K. 1987 Water stress on leaf elongation, leaf water potential, transpiration and nutrient uptake of rice, maize and soybean. *Plant and Soil* **103**, 155–168.
- Tucker, C. J. 1979 Red and photographic infrared linear combination for monitoring vegetation. *Remote Sens. Environ.* **8**, 127–150.
- Wan, Z. & Li, Z. L. 1997 A physics-based algorithm for retrieving land-surface emissivity and temperature from EOS/MODIS data. *IEEE Trans. Geosci. Remote Sens.* **35**, 980–996.
- Weckwerth, T. M., Parsons, D. B., Koch, S. E., Moore, J. A., LeMone, M. A., Demoz, B. B., Flamant, C., Geerts, B., Wang, J. & Feltz, W. F. 2004 An overview of the International H₂O Project (IHOP_2002) and some preliminary highlights. *Bull. Am. Meteorol. Soc.* **85**(2), 253–277.
- Weiss, J. L., Gutzler, D. S., Coonrod, J. E. A. & Dahm, C. N. 2004 Seasonal and inter-annual relationships between vegetation and climate in central New Mexico, USA. *J. Arid Environments* **57**, 507–534.
- Zeng, X., Dickinson, R. E., Walker, A. & Shaikh, M. 2000 Derivation and evaluation of global 1-km fractional vegetation cover data for land modeling. *J. Appl. Meteorol.* **39**, 826–839.